VII International Conference on Computational Methods in Marine Engineering
MARINE 2017
M. Visonneau, P. Queutey and D. Le Touzé (Eds)

SIMULATION OF BREAKING FOCUSED WAVES OVER A SLOPE WITH A CFD BASED NUMERICAL WAVE TANK

MAYILVAHANAN ALAGAN CHELLA[1*], HANS BIHS[1], CSABA PÁKOZDI[2], DAG MYRHAUG[3] AND ØIVIND ASGEIR ARNTSEN [1]

[1] Department of Civil and Environmental Engineering, NTNU
Trondheim, Norway

[2] SINTEF Ocean
[3] Department of Marine Technology, NTNU
Trondheim, Norway

Key words: Numerical simulation, Focused waves, Breaking waves, Single flap maker, Breaking waves

Abstract. Extreme wave conditions are always identified with large-amplitude breaking waves in shallow waters. Focused waves can often be used to describe extreme waves which evolve during the nonlinear wave-wave interaction, occurring at one point in space and time. Understanding breaking focused waves has many design-related implications for the design of offshore wind turbine (OWT) substructures in shallow waters. The main objective of the paper is to model breaking focused waves over a sloping seabed and study the breaking characteristics using the open-source CFD model REEF3D. The numerical model describes the two-phase flow using the incompressible Reynolds-Averaged Navier-Stokes (RANS) equations together with the continuity equation. The model uses a fifth-order WENO scheme for convection discretization and a third order Runge-Kutta scheme for time discretization along with the level set method to obtain the free surface, yielding accurate wave propagation in the numerical wave tank. Solid boundaries are accounted through the ghost cell immersed boundary method. The free surface is modeled with the level set method. Turbulence is described with the two-equation $k-\omega$ model. In the numerical wave tank, the focused waves are generated using a single flap-type maker theory. The numerical results are in good agreement with experimental results for complex free surface elevations measured at several locations along the wave tank. The numerical aspects related to the development of the breaking process are investigated together with the evolution of focusing wave group in the numerical wave tank. Further, the study also examines the free surface flow features that evolve during the breaking process.

1 INTRODUCTION

Hydrodynamic loads from extreme waves on offshore wind turbine substructures is an important design criterion [1]. Extreme waves are characterized by a single large steep wave crest

with high degree of asymmetry. They are much larger than expected for the normal sea state. Despite that the extreme events are exceptional events, they can cause severe damage to offshore structures. Considering the nonlinear behavior of shallow water waves, the shortening of wave length resulting in larger wave heights. In addition to the strong wave-wave interactions, the waves are affected by the seabed bathymetry. This causes the drastic changes in the wave transformation characteristics. The extreme waves events can be modelled with focused waves which are results of superposition of many linear wave components concentrating at the intended space and time.

Waves grow steeper and higher and they break more frequently in shallow waters. The interaction of breaking waves with offshore structures exerts severe hydrodynamic loading on them. There have been limited studies on these engineering aspects relevant to the hydrodynamic load assessment parameters in shallow waters, especially for breaking focused waves over a sloping seabed. Despite several numerical studies based on comoutational fluid dynamics (CFD) have been carried out to model non-breaking focused waves over constant depth [2, 3, 4, 5, 6, 7], there have been limited numerical studies on focused waves over slopes, particularly breaking focused waves. In addition, the breaking characteristics of focused waves over a slope are not yet fully understood due to many parameters involved in the physical processes. It is quiet challenging to describe the evolution of a focused wave group over a slope since the focusing mechanism needs to be defined along with other physical processes such as shoaling and breaking.

The main purpose of the present paper is to simulate breaking focused waves over a slope and investigate the breaking characterisctics with the open-source CFD model REEF3D [8]. First, the numerical model is validated by comparing the computed results with experimental data for wave surface elevations along the wave tank. A good agreement between the numerical results and experimental data is obtained. Further, the numerical aspects related to the development of the breaking process are investigated together with the evolution of focusing wave group in the numerical wave tank. The prominent free surface flow features evolve during the breaking process is also presented and discussed.

2 NUMERICAL MODEL

In the open-source CFD model REEF3D, the unsteady Reynolds-Averaged Navier Stokes (URANS) equations along with the continuity equation are solved for incompressibe two-phase flow in the numerical wave tank[8]. The mass and momentum equations are:

$$\frac{\partial u_i}{\partial x_i} = 0 \tag{1}$$

$$\frac{\partial u_i}{\partial t} + u_j \frac{\partial u_i}{\partial x_j} = -\frac{1}{\rho}\frac{\partial p}{\partial x_i} + \frac{\partial}{\partial x_j}\left[(\nu + \nu_t)\left(\frac{\partial u_i}{\partial x_j} + \frac{\partial u_j}{\partial x_i}\right)\right] + g_i \tag{2}$$

Here, u is the mean velocity components, p is the pressure, ρ is the fluid density, ν is the kinematic viscosity, ν_t is the eddy viscosity, i and j denote the indices in x and y direction, respectively and g_i is the gravity term. The discretization of convective terms of the URANS equations are treated with the fifth-order weighted essentially non-oscillatory (WENO) scheme [9] which is a higher order conservative finite difference scheme. For the time integration, the third-order accurate TVD Runge-Kutta scheme [10] is implemented. The time step determination is based on an

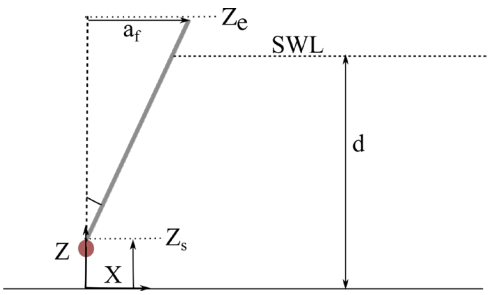

Figure 1: A definition sketch of flap wave maker

adaptive time stepping method [11] which is controlled by the Courant-Friedrichs-Lewy (CFL) criterion. The CFL criterion is maintained and the simulation time step is adjusted for each iteration. This method accounts for the effects of velocity and the source term S on the temporal numerical solutions. Moreover, this approach enhances the robustness of the numerical model, the overall efficiency and the credibility of simulation results. The pressure term in URANS equation is modeled with the Chorins projection method [12]. First, the intermediate velocity is calculated without considering the pressure gradient term in the URANS equation. Next, with the intermediate velocity field, the pressure is calculated from the Poisson equation using the Jacobi-preconditioned BiCGStab solver [13]. Finally, the pressure term is used to update the velocity field. In addition, the implementation of staggered grid method ensures a tight coupling between pressure and velocity fields.
The free surface computations are performed with the level set method. It is defined as the signed distance function $\phi(\vec{x}, t)$ [14] and it provides the distance to the interface and also the sign as follows:

$$\phi(\vec{x}, t) \begin{cases} > 0 \; if \; \vec{x} \in water \\ = 0 \; if \; \vec{x} \in \Gamma \\ < 0 \; if \; \vec{x} \in air \end{cases} \tag{3}$$

A convection equation for the level set function is:

$$\frac{\partial \phi}{\partial t} + u_j \frac{\partial \phi}{\partial x_j} = 0 \tag{4}$$

The Eikonal equation $|\nabla \phi| = 1$ is valid in the computational domain. The URANS equations are closed with the two-equation $k - \omega$ model [15]. A three-dimensional ghost cell immersed boundary method (GCIBM) [16] is implemented to model the complex geometries. Parallel computation based on the domain decomposition method and MPI (Message passing interface) is implemented in the numerical model.

2.1 Wave generation

In the laboratory experiments performed by Svangstu (2011) [17], a flap-type wave generator was used to generate focused waves. In order to mimic the experimental condition, a single hinged flap-type wave maker theory is implemented in the numeral model. In the numerical

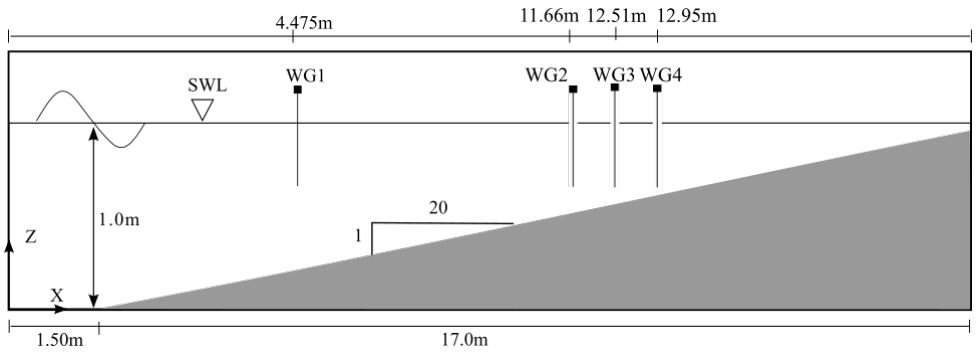

Figure 2: Numerical set-up

wave tank, focused waves are generated using the recorded time history of paddle motion of the physical wave flume. A flap wave maker is hinged at a distance of z_s=0.06m from the bottom with a height of z_e=1.36m and it corresponds to rotating angle (θ) as shown in Fig. 1. At the undisturbed free surface (z=0), the flap horizontal displacement is x_f and the velocity is u_f. The horizontal displacement (x_f) of a flap decreases linearly towards the hinge point at which the displacement is zero.

$$x_f = \frac{z - z_s}{z_e - z_s} a_f |sin\theta| \tag{5}$$

The angle θ and a_f are related as follows:

$$tan\theta = \frac{a_f}{z_e - z_s} \tag{6}$$

At the outlet boundary, the active beach [18] is implemented to absorb waves. REEF3D [8] has been used to study a wide range of coastal and offshore problems. The numerical model is well utilized for modelling breaking waves in shallow waters [19, 20], non-breaking and breaking wave interaction with vertical cylinders[21, 22, 23, 24].

3 RESULTS AND DISCUSSION

3.1 Numerical set-up and grid refinement study

The numerical set-up consists of a 1.5m long flatbed followed by a slope of 1/20 with a water depth of 1.0m. as shown in Fig. 2. The coordinate system is the same as the laboratory experiments. The wave maker consists of a paddle of 1.36 m long that is hinged (at z=0.06m) on a raised support structure. At the wave inlet, the measured time history of paddle displacement is given as input to generate focused waves. In order to examine the effect of grid size on the numerical results, three grid sizes, dx=0.01m, 0.025m and 0.05m are tested in the present study. Fig. 3 show the comparison of experimental and numerical wave surface elevations at x=4.75m (WG1) and 12.21m (WG3) for different grid sizes dx=0.01m, 0.025 and 0.05m. The computed focused wave crest with dx 0.05m at both wave gauges are lower and the phases are also different than the experimental data 3. The numerical results with dx=0.01m and 0.025m show good agreement with the measured data at both wave gauges. Though with dx=0.01m, the

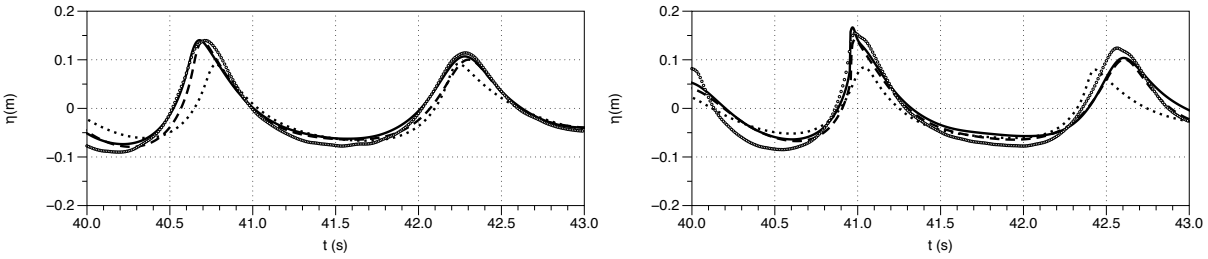

(a) x=4.75m (WG1) (b) x=12.21m (WG3)

Figure 3: Grid refinement study for dx=0.01m (solid lines), 0.025m (dashed lines) and 0.05m (dotted lines). Circles: experimental data [17].

experimental waves are accurately represented including the asymmetric focused wave profile before breaking at x=12.21m (WG3). Therefore the grid size dx=0.01m is considered for the present study.

3.2 Breaking focused wave characteristics

Focused waves are generated using a single hinged flap maker theory as discussed in Sec. 2.1. Fig. 4 shows comparison of numerical results with the experimental data for the wave surface elevations along the wave tank at x=4.75m (a, WG1), 11.66m (b, WG2), 12.51m (c, WG3) and 12.95m (WG4). It appears that the computed wave surface elevations are in good agreement with the measured results for all wave gauges. When the focused wave group propagates over the slope in decreasing water depth, the focused as well as the secondary wave crests transform into narrower and sharper due to shoaling which causes the shallow water steepening and shortening of waves. At x=4.75m, the focused wave group are started to shoal without much deformations. During the initial stages of shoaling, potential energy slightly increases as the wave height increases and thus, kinetic energy slightly decreases.

As the wave group propagates further over the slope, the speed of the wave group is retarded and the wave height further increases at x=11.66m (WG2). The wave group consists of a number of waves of different frequencies are started superimposing upon each other causing a single large focused wave crest as shown in Fig. 4 (b) x=11.66m (WG2) and (c) 12.51 (WG3). When the focused wave crest reaches the maximum height, particle velocity in the upper part of the wave crest increases and thus, kinetic energy. Finally, the steep wave front becomes nearly vertical and eventually the main focused wave crest breaks. Fig. 4 (d) shows the free surface elevation of a nearly breaking wave crest at x=12.51m (WG3). In the laboratory experiments, the focused wave crest breaks between x12.51m (WG3) and 12.91m (WG4) as the exact breaking location is not available. Whereas in the numerical simulation, the wave breaks exactly at x_b=12.62m. The computed breaker water depth (d_b) and the breaker height are 0.46m and 0.22m, respectively. As expected, the computed focused wave height decreases after breaking as presented in Fig. 4 (e) due to energy loss during breaking. Moreover, the computed free surface elevations during shoaling, breaking and post-breaking stages are in good agreement with the experimental data.

Fig. 5 shows comparison of numerical free surface profiles with the experimental data for the

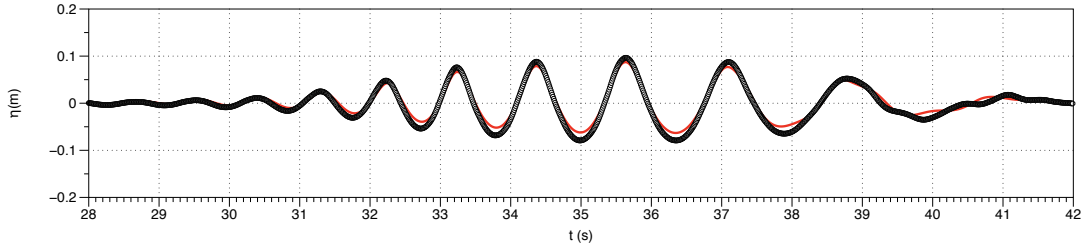

(a) x=4.75m (WG1)

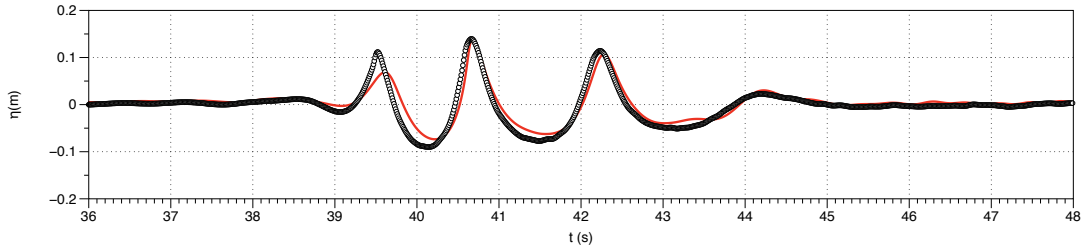

(b) x=11.66m (WG2)

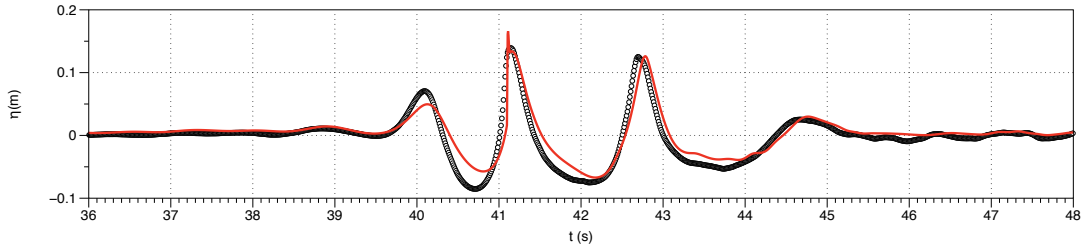

(c) x=12.51m (WG3)

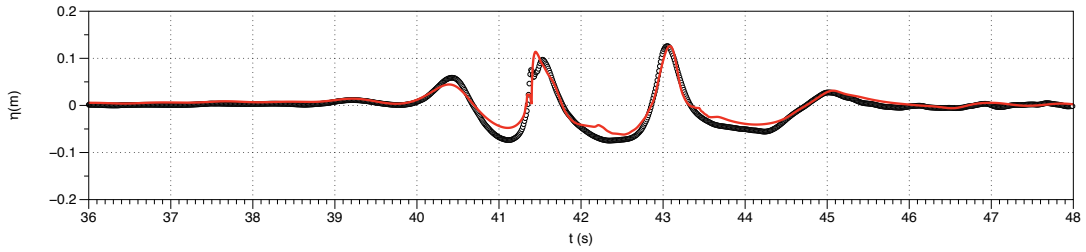

(d) x=12.95m (WG4)

Figure 4: Computed wave surface elevations along the wave tank at x=4.75m (WG1), 11.66m (WG2), 12.21m(WG3), 12.51m (WG4) and 12.95m (WG5); circles: experimental data [17] and red solid lines: numerical results.

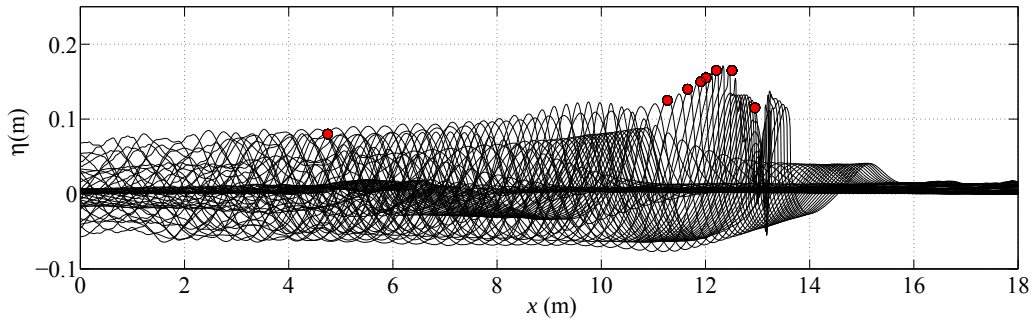

Figure 5: Evolution of free surface elevations at different time instants along the wave tank; black solid lines: numerical results and red circles: experimental data [17].

evolution of the focused wave group along the wave tank. The wave components start to focus as the group propagates over the slope and the amplitude of the focused wave crest increases. The focus wave height increases continuously up to the breaking point and the focused wave crest breaks at x_b=12.62m. After the breaking point, the wave heights suddenly decreases shoreward. The propagation of the wave group and the development of the focused wave crest during shoaling and breaking are consistent with the experimental data[17].

3.3 Free surface flow features of breaking focused waves

Fig. 6 presents the simulated free surface profiles with velocity magnitude (m/s) at t=41.45s, 41.80s, 41.90s and 42.0s after breaking. As mentioned in Sec 3.2, the focused wave crest evolved from the wave group breaks at x=12.62m with a large wave front. At the incipient of breaking, the front face of the focused wave crest becomes vertical. As the wave group propagates further over the slope the upper part of the focused wave crest with high velocity travels faster than the rest of the wave. The wave front overturns and ejects forward in the wave direction as shown in Fig. 6 (a) and (b). Then the overturned wave crest falls down into the forward wave trough and causes a enclosed air-pocket as shown in Fig. 6 (c). Further the translation of the overturned crest displaces a portion of water shoreward causing the splash-up and the formation of secondary waves crest as depicted in Fig. 6 (d). It should be noted that the velocity magnitude of the secondary wave crest is almost equal to the velocity of the main wave crest. The simulated flow features such as the development of overturning wave crest and its impingement and the formation of air-pocket, the splash-up and the secondary wave crest are well captured in the present numerical simulations. Moreover, the numerically captured free surface flow features are consistent with the previous numerical studies [**?**, 20] and experimental studies [**?**, **?**] on breaking waves over slopes.

4 CONCLUSIONS

Breaking focused waves are simulated in the numerical wave tank based on the CFD model REEF3D. The numerical model describes the two-phase flow using the incompressible Reynolds-Averaged Navier-Stokes (RANS) equations together with the continuity equation. The free

surface is modeled with the level set method. Turbulence is described with the two-equation $k-\omega$ model. The computed results are compared with the experimental data for wave surface elevations over the slope and the development of the free surface profiles along the wave tank during the breaking process. The experimental and theoretical comparison showed to be in a good agreement. Further, the transformation of the focused wave group over a slope is also presented and discussed. The simulated free surface flow features are consistent with the previous studies on regular breaking waves over slopes. The present numerical study provides some insight into the modeling aspects of breaking focused waves and the physical processes related to the evolution of breaking focused waves over a sloping seabed. The present work has investigated some aspects concerning the characteristics of breaking focused waves. However, more research is needed to understand the complete physical processes involved during the interaction of breaking focused waves with structures and the related flow characteristics including the wave impact forces.

5 ACKNOWLEDGMENT

The research work has been funded by the Research Council of Norway through the project "Hydrodynamic Loads on Offshore Wind Turbine Substructures due to Nonlinear Irregular Breaking, High Steep and Extreme Waves" (project number: 246810). The authors gratefully acknowledge the computing time granted by NOTUR (project number: NN2620).

REFERENCES

[1] Alagan Chella, M., Tørum, A., and Myrhaug, D., 2012. "An overview of wave impact forces on offshore wind turbine substructures". *Energy Procedia,* ***20***, pp. 217–226.

[2] Ning, D. Z., Zang, J., Liu, S. X., Eatock Taylor, R., Teng, B., and Taylor, P. H., 2009. "Free-surface evolution and wave kinematics for nonlinear uni-directional focused wave groups". *Ocean Engineering,* ***36***, pp. 1226—1243.

[3] Westphalen, J., Greaves, D. M., Williams, C. J. K., Hunt-Raby, A. C., and Zang, J., 2012. "Focused waves and wave-structure interaction in a numerical wave tank". *Ocean Engineering,* ***45***, pp. 9–21.

[4] Bihs, H., Alagan Chella, M., , Kamath, A., and Arntsen, Ø. A., 2016. "Wave-structure interaction of focussed waves with reef3d". In Proceedings of the 35-th International Conference on Offshore Mechanics and Arctic Engineering.

[5] Ning, D. Z., Teng, B., Eatock Taylor, R., and Zang, J., 2008. "Numerical simulation of non-linear regular and focused waves in an infinite water-depth". *Ocean Engineering,* ***35***, pp. 887—899.

[6] Bai, W., and Eatock Taylor, R., 2007. "Numerical simulation of fully nonlinear regular and focused wave diffraction around a vertical cylinder using domain decomposition". *Applied Ocean Research,* ***29***, pp. 55–71.

[7] Pakozdi, C., Kendon, T. E., Stansberg, C. T., and Arntsen, Ø. A., 2012. "A numerical study of a focused wave packet near the surf zone". In Proceedings of the 31-st International Conference on Offshore Mechanics and Arctic Engineering.

[8] Bihs, H., Kamath, A., Alagan Chella, M., Aggarwal, A., and Arntsen, Ø. A., 2016. "A new level set numerical wave tank with improved density interpolation for complex wave hydrodynamics". *Computers and Fluids,* ***140***, pp. 191–208.

[9] Jiang, G. S., and Shu, C. W., 1996. "Efficient implementation of weighted ENO schemes". *J. Comput. Phys.,* ***126***, pp. 202–228.

[10] Shu, C. W., and Osher, S., 1988. "Efficient implementation of essentially non-oscillatory shock capturing schemes". *J. Comput. Phys.,* ***77***, pp. 439–471.

[11] Griebel, M., Dornseifer, T., and Neunhoeffer, T., 1998. *Numerical Simulation in Fluid Dynamics, a Practical Introduction.* SIAM.

[12] Chorin, A., 1968. "Numerical solution of the Navier-Stokes equations". *Math. Comput.,* ***22***, pp. 745–762.

[13] van der Vorst H., 1992. "Bi-CGSTAB: A fast and smoothly converging variant of Bi-CG for the solution of nonsymmetric linear systems". *SIAM Journal on scientific and Statistical Computing,* ***13***, pp. 631–644.

[14] Osher, S., and Sethian, J. A., 1988. "Fronts propagating with curvature-dependent Speed: Algorithms based on Hamilton-Jacobi formulations". *J. Comput. Phys.,* ***79***, pp. 12–49.

[15] Wilcox, D. C., 1994. *Turbulence Modeling for CFD.* DCW Industries Inc., La Canada, California.

[16] Berthelsen, P. A., and Faltinsen, O. M., 2008. "A local directional ghost cell approach for incompressible viscous flow problems with irregular boundaries". *J. Comput. Phys.,* ***227***, pp. 4354–4397.

[17] Svangstu, E., 2011. "An investigation of wave conditions and wave induced loads for design of wind turbine foundations at 15-40m depth.". Master's thesis, NTNU Trondheim.

[18] Schäffer, H. A., and Klopman, G., 2000. "Review of multidirectional active wave absorption methods". *J. Waterw. Port Coast. Ocean Eng.,* ***126***, pp. 88–97.

[19] Alagan Chella, M., Bihs, H., and Myrhaug, D., 2015b. "Characteristics and profile asymmetry properties of waves breaking over an impermeable submerged reef". *Coast. Eng.,* ***100***, pp. 26–36.

[20] Alagan Chella, M., Bihs, H., Myrhaug, D., and Muskulus, M., 2016. "Hydrodynamic characteristics and geometric properties of plunging and spilling breakers over impermeable slopes". *Ocean Modelling,* ***103***, pp. 53–72.

[21] Kamath, A., Alagan Chella, M., Bihs, H., and Arntsen, Ø. A., 2015. "CFD investigations of wave interaction with a pair of large tandem cylinders". *Ocean Eng.,* ***108***, pp. 734–748.

[22] Kamath, A., Alagan Chella, M., Bihs, H., and Arntsen, Ø. A., 2016. "Breaking wave interaction with a vertical cylinder and the effect of breaker location". *Ocean Eng.,* ***128***, pp. 105–115.

[23] Bihs, H., Kamath, A., Alagan Chella, M., and Arntsen, Ø. A., 2016. "Breaking wave interaction with tandem cylinders under different impact scenarios". *J. Waterw. Port Coast. Ocean Eng.* DOI: 10.1061/(ASCE)WW.1943-5460.0000343.

[24] Alagan Chella, M., Bihs, H., Myrhaug, D., and Muskulus, M., 2017. "Breaking solitary waves and breaking wave forces on a vertically mounted slender cylinder over an impermeable sloping seabed". *Journal of Ocean Engineering and Marine Energy,* ***3***, pp. 1–19.

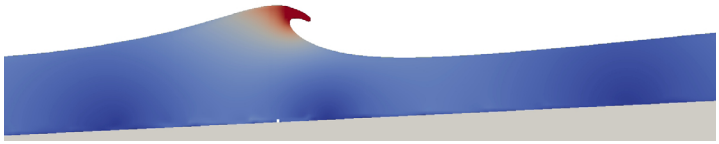

(a) t=41.45s

(b) t=41.80s

(c) t=41.90s

(d) t=42.00s

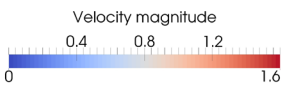

Figure 6: Free surface flow features with velocity magnitude after breaking for different time instants at t= 41.45s (a), 41.80s (b), 41.90s (c) and 42.0s (d).